TISSUE ENGINEERING: Part C
Volume 19, Number 4, 2013

DOI: 10.1089/ten.tec.2012.0287

Tissue-Engineered Constructs of Human Oral Mucosa Examined by Raman Spectroscopy

Alexander Khmaladze,[1] Arindam Ganguly,[1] Shiuhyang Kuo,[2,3] Mekhala Raghavan,[1] Raghu Kainkaryam,[4] Jacqueline H. Cole,[1] Kenji Izumi,[5] Cynthia L. Marcelo,[2,3] Stephen E. Feinberg,[2,3] and Michael D. Morris[1]

A noninvasive quality monitoring of tissue-engineered constructs is a required component of any successful tissue-engineering technique. During a 2-week production period, *ex vivo* produced oral mucosa-equivalent constructs (EVPOMEs) may encounter adverse culturing conditions that might compromise their quality and render them ineffective. We demonstrate the application of near-infrared Raman spectroscopy to *in vitro* monitoring of EVPOMEs during their manufacturing process, with the ultimate goal of applying this technology *in situ* to monitor the grafted EVPOMEs. We identify Raman spectroscopic failure indicators for less-than optimal EVPOMEs that are stressed by higher temperature and exposure to higher than normal concentration of calcium ions. Raman spectra of EVPOMEs exposed to thermal and calcium stress showed correlation of the band height ratio of CH_2 deformation to phenylalanine ring breathing modes, providing a Raman metric to distinguish between viable and nonviable constructs. We compared these results to histology and glucose consumption measurements, demonstrating that Raman spectroscopy is more sensitive and specific to changes in proteins' secondary structure not visible by H&E histology. We also exposed the EVPOMEs to rapamycin, a cell growth inhibitor and cell proliferation capacity preserver, and distinguished between EVPOMEs pretreated with 2 nM rapamycin and controls, using the ratio of the Amide III envelope to the phenylalanine band as an indicator.

Introduction

Tissue engineering[1] is becoming a viable technique for organ and tissue reconstruction in humans.[2] In oral and maxillofacial surgery, soft tissue-engineered constructs are needed to solve issues related to a deficiency in sufficient oral mucosa for intraoral grafting procedures. Oral mucosal grafts are essential for use in various applications, including preprosthetic surgery, dental implants, and oral reconstructions due to trauma, oral cancer, or congenital defects. Since oral mucosa is in short supply, alternatives such as a skin graft are used that require harvesting of tissue from secondary sites, leading to additional donor-site morbidity.[3] In addition, split-thickness skin grafts do not always have acceptable mechanical properties due to their different keratinization pattern.[4] To overcome these limitations, a tissue-engineering approach has been applied to the fabrication of skin and mucosal substitutes.[5–9] An example of such a substitute is the human *ex vivo* produced oral mucosa-equivalent constructs (EVPOMEs),[3,10–12] which hold multiple advantages, such as excellent handling characteristics and production in a serum-free defined culture medium without a feeder layer (eliminating the danger of transferring xenogenous components to the cocultured autologous cells[6]). The EVPOME has been used in a Food and Drug Administration (FDA)-approved human clinical trial.[12]

One of the challenges currently faced by tissue-engineered constructs is that most of these cell-based products require continuous monitoring to assess cell viability and metabolic function.[13] There is a number of bioanalytical techniques available to monitor the production of these constructs; however, these techniques are costly, invasive, and require sophisticated specimen preparation.[14,15]

In comparison, Raman spectroscopy offers a simple, noninvasive, and rapid method to monitor the quality of the tissue-engineered constructs during and at the end of their manufacturing process. Raman spectroscopy has been already effectively employed to provide biochemical information in cells and tissues[16–19] and can also be used on tissue-engineered constructs.[20–22] In this article, we demonstrate the utility of

[1]Department of Chemistry, University of Michigan, Ann Arbor, Michigan.
[2]Department of Oral and Maxillofacial Surgery, School of Dentistry, University of Michigan, Ann Arbor, Michigan.
[3]Department of Surgery, University of Michigan, Ann Arbor, Michigan.
[4]Cincinnati, Ohio.
[5]Department of Oral Anatomy, Graduate School of Medical and Dental Sciences, Niigata University, Japan.

Raman spectroscopy for monitoring EVPOMEs during their fabrication *in vitro*. In particular, we identify Raman spectroscopic metrics, which serve as EVPOME failure indicators, as well as a metric that distinguishes EVPOMEs pretreated with rapamycin, a chemical that is capable of affecting cell behavior.[23]

Rapamycin[24] possesses immunosuppressive, antifungal, and antitumor properties. It also functions as a cell-rejuvenating reagent and can preserve cell proliferation capacity and enhance cell longevity.[25] It is expected that rapamycin pretreatment of oral keratinocytes may increase EVPOME viability and alter its function.

Materials and Methods

Materials

The procedures for harvesting human oral mucosal tissue were approved by the University of Michigan Institutional Review Board. The methods for culturing primary human oral keratinocytes and EVPOMEs were detailed previously.[3,11] In short, primary human oral keratinocytes were enzymatically dissociated from discarded oral mucosa tissues. The cell cultures were established in a chemically defined culture medium (EpiLife and EDGS; Invitrogen, Life Technologies) containing 0.06 mM calcium, 25 μg/mL gentamicin, and 0.375 μg/mL fungizone (Invitrogen, Life Technologies). To produce a single EVPOME, 2×10^5 cells/cm^2 were seeded on a 1-cm^2 acellular cadaver dermis (AlloDerm®; LifeCell Corp.), which was presoaked in 5 μg/cm^2 human type IV collagen (Sigma). Cells and AlloDerm substrates were immersed in a medium containing 1.2 mM calcium for 4 days and then raised to an air–liquid interphase for additional 7 days to allow cell stratification. Nonstressed EVPOMEs were produced at 37°C. Thermally stressed batches were maintained at 43°C overnight on day 9 postseeding for 24 h and switched back to 37°C for 24 h before analysis. Calcium-stressed EVPOMEs were cultured in a medium containing a higher-than-normal concentration of Ca^{2+} ions. For rapamycin studies, cells were grown in a medium containing 0.06 mM calcium and 2 nM rapamycin for 5 days before we used them to manufacture EVPOMEs. EVPOMEs for rapamycin experiments were cultured in 1.2 mM calcium either without rapamycin or in the presence of 2 nM rapamycin. At day 11 postseeding, EVPOME samples were collected, fixed with 10% formalin, and embedded in paraffin for histological examination. Specimens were cut into 5-μm sections and stained with hematoxylin and eosin. Histology samples were processed by The Dental School Histology Core Facility.

Typical cross-sections of AlloDerm substrates and EVPOMEs are shown in Figure 1. The thickness of AlloDerm and the keratinized layer formed on top varies from specimen to specimen. (The partial disruption of the cellular layer with thermal stress and a more gradual disruption of the cellular level with the increased concentration of calcium can be observed.) Since a 4×/0.2 NA objective was used in these experiments (see below), the spectral features of EVPOME reported here included contributions from both the AlloDerm substrate and the cellular layer above it.

Raman spectroscopy

Raman spectra were obtained using a locally constructed Raman microscope. The system (previously described[26]) is

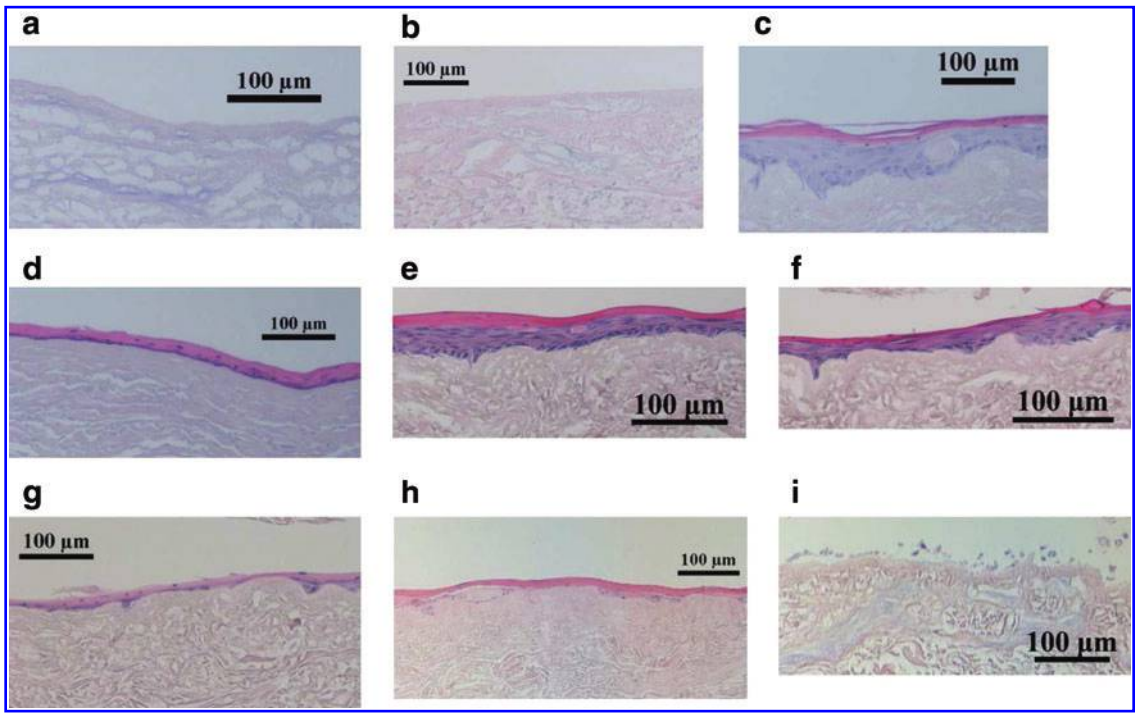

FIG. 1. Images of cross-sections of specimens: **(a)** nonstressed AlloDerm®, **(b)** thermally stressed AlloDerm, **(c)** nonstressed *ex vivo* produced oral mucosa-equivalent constructs (EVPOMEs), and **(d)** thermally stressed EVPOMEs. EVPOMEs cultured in a medium containing **(e)** 1.2 mM of Ca^{2+} ions, **(f)** 1.8 mM of Ca^{2+} ions, **(g)** 2.4 mM of Ca^{2+} ions, **(h)** 3.0 mM of Ca^{2+} ions, and **(i)** 4.0 mM of Ca^{2+} ions. Scale bar is 100 μm. Color images available online at www.liebertpub.com/tec

built around an epifluorescence microscope (Nikon E600). A line-focused 785-nm laser (Invictus; Kaiser Optical Systems, Inc.), focused through a 4X/0.2 NA objective, generated laser power of 120–130 mW at the specimen. The signal was collected through the same objective, transmitted toward, and focused into an imaging spectrograph (HoloSpec; Kaiser Optical Systems, Inc.). Raman spectra were collected through 25-μm and 50-μm slits, yielding an approximate spectral resolution of 4 and 8 cm^{-1}, respectively. The spectra were recorded by a 1024×256 pixel deep-depletion charge-coupled device detector (Model DU 401-BR-DD; Andor Technology). The wavelength-dependent response of the detector and the wavelength scale of the spectrograph were calibrated using a HoloSpec Calibration Accessory (Kaiser Optical Systems, Inc.). Each spectrum was corrected for spectrograph image curvature, white-light corrected, dark-current subtracted, and baseline adjusted by a modified polyfit method.[27]

In this study, we used a 4×/0.2 NA objective, which was intended to approximate the depth penetration of 0.22 NA multimode optical fibers that are commonly used in fiber-optic Raman probes. This was done in preparation to employing this technique to monitor the incorporation of EVPOMEs *in situ* into mice and eventually into human subjects.

Data collection

Measurements were made on multiple EVPOMEs and AlloDerm control batches (each batch corresponding to a single donor), with specimens from each batch studied on the same day under the same conditions. For stressed-versus-nonstressed experiments, the specimens from each batch included stressed (either thermal or Ca^{2+}) and nonstressed EVPOMEs and AlloDerm controls. For rapamycin experiments, the batches included rapamycin-treated EVPOMEs and untreated EVPOME controls. EVPOME and AlloDerm specimens were mounted on sapphire flats. Spectral transects (~100 μm in length) were collected at multiple locations on each specimen and averaged to give a single spectrum for the specimen. Each batch contained a total of 20–30 specimens of EVPOMEs and AlloDerm controls.

Data analysis

Raman bands were fitted by the Levenberg–Marquardt algorithm. Singular value decomposition (SVD) analysis[28] and fits were performed in Labview. *T*-tests were performed to evaluate the ability of Raman metrics to discriminate between the stressed and nonstressed status. Differences were considered significant at $p<0.05$. A threshold value was determined for the most significant Raman metrics to obtain better separation between stressed and nonstressed samples or between damaged and intact samples. Sensitivity and specificity were calculated according to a standard formula.

Results

In this study, both EVPOMEs and AlloDerm substrates without cells (controls) were subjected to two kinds of stress: (1) thermal by keeping the specimens at 43°C overnight on day 9, which induced temperature damage on cell growth and EVPOME development and (2) calcium by exposing specimens to various higher-than-normal concentrations of Ca^{2+} ions, which altered physiological development of the cells.

Thermal stress

The average Raman spectra of thermally stressed and nonstressed EVPOME and AlloDerm (collected from

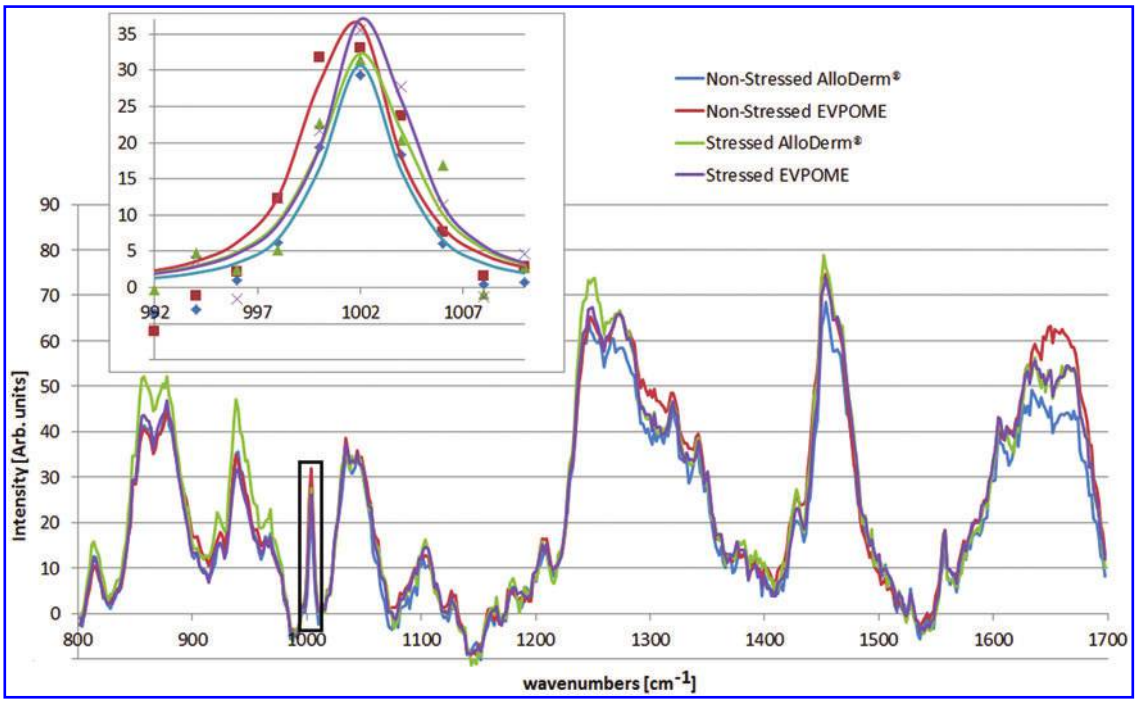

FIG. 2. Raman spectra of thermally stressed and nonstressed EVPOMEs and AlloDerm. Phenylalanine at 1004 cm^{-1}, broad amide III band at 1250 cm^{-1}, CH_2 at 1450 cm^{-1}, and amide I at 1650 cm^{-1} bands are clearly visible. The inset shows the phenylalanine band. Color images available online at www.liebertpub.com/tec

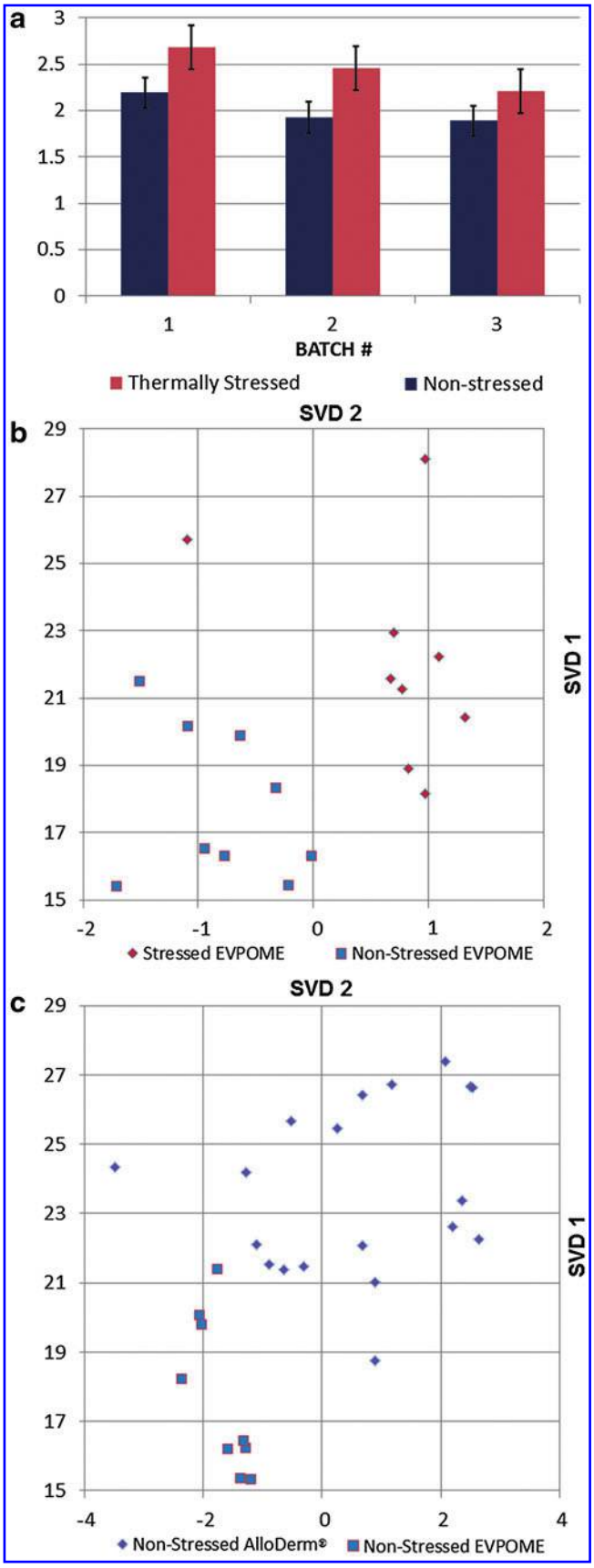

specimens shown in Fig. 1) are shown in Figure 2. Four major bands are seen: phenylalanine ring breathing mode at 1004 cm^{-1}; amide III envelope, maximum at 1250 cm^{-1}; CH_2 deformation at 1450 cm^{-1}; and amide I envelope, maximum at 1650 cm^{-1}. The phenylalanine band is sharp and contains only one band, allowing for a relatively straightforward band fitting (see inset). The structure of the CH_2 deformation band is more complex, and both amide I and amide III envelopes contain multiple overlapping unresolved bands. Since all of the spectra in Figure 2 were collected under similar conditions, the intensities of the bands could be compared without normalizing.

The CH_2/phenylalanine band ratios for thermally stressed and nonstressed EVPOMEs for three batches are shown in Figure 3a. We observed batch effects, which may be caused by factors such as variable thickness of AlloDerm substrates and different cellular layer quality because of small variations in execution of the production protocol and patient-specific variability in cell activity, as primary cell strains were used. While the individual CH_2/phenylalanine band ratios were not the same for each batch, the ratio of stressed to nonstressed EVPOMEs for the CH_2/phenylalanine band ratios was consistent. CH_2/phenylalanine band ratios were always about 20% greater for thermally stressed than for nonstressed EVPOMEs ($p = 0.045$).

Shape changes in the amide bands also occurred as a result of thermal stressing. Such changes along with band intensity information can be visualized using multivariate techniques. We have found that SVD applied to our data (see Fig. 3b) showed clear separation between stressed and nonstressed EVPOMEs. Furthermore, the SVD principal component plot comparing AlloDerm and EVPOMEs (Fig. 3c) distinguished between areas of EVPOME where the cell layer is severely disrupted and where it is intact.

Calcium stress

Raman spectra of EVPOMEs exposed to four different concentrations of Ca^{2+} ions are shown in Figure 4. The lowest concentration is considered physiologically normal, and thus the construct is assumed to be nonstressed. The Raman spectra were normalized to the phenylalanine band to help visualize the CH_2/phenylalanine band intensity ratios for different concentrations. Major differences were seen in the amide I and amide III regions, especially for higher Ca^{2+} ion concentrations.

Batch effects were again observed (Fig. 5a). Figure 5b shows the CH_2/phenylalanine band ratios for different concentrations averaged across batches. The ratio was always higher for stressed than for nonstressed specimens ($p = 0.03$). At higher concentrations, the variation was greater (as indicated by larger error bars). The ratios of CH_2 to phenylalanine bands were consistently higher for Ca^{2+}-

FIG. 3. Thermal stressing of EVPOME. **(a)** The ratio of CH_2 to phenylalanine band heights for three available batches of thermally stressed and nonstressed EVPOMEs. The results of singular-value decomposition (SVD) analysis, showing clear separation: **(b)** thermally stressed versus nonstressed EVPOMEs and **(c)** thermally nonstressed AlloDerm substrate versus nonstressed EVPOMEs. Color images available online at www.liebertpub.com/tec

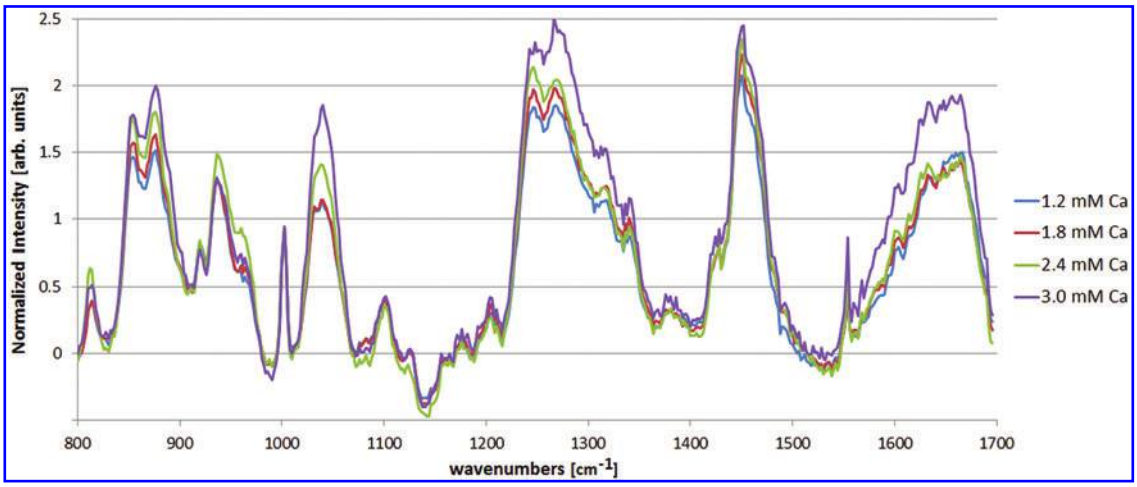

FIG. 4. Normalized Raman spectra of EVPOMEs stressed by various concentrations of calcium ions. The spectra are normalized to phenylalanine for consistency and to allow fitting to a well-defined band. Color images available online at www.liebertpub.com/tec

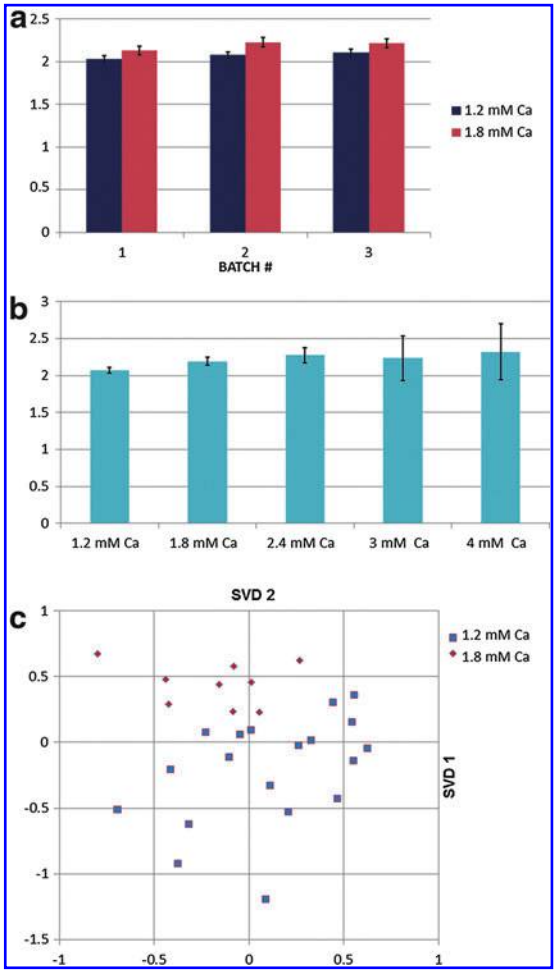

FIG. 5. Ca^{2+} ion stressing. The ratio of CH_2 to phenylalanine band heights for **(a)** 3 available batches of stressed and nonstressed EVPOMEs, **(b)** higher concentrations of Ca^{2+} stressing (averages across batches), and **(c)** SVD of Ca^{2+} stressing. Color images available online at www.liebertpub.com/tec

stressed specimens, although the difference between the stressed and the nonstressed (5%–7%) was not as large as in the case of thermal stressing (see Fig. 3a). Finally, Figure 5c shows that the results of SVD analysis showed separation of Ca^{2+}-stressed and nonstressed EVPOME spectra.

Rapamycin treatment

We also investigated Raman spectral changes resulting from pretreatment of the human keratinocytes with rapamycin. The averaged Raman spectrum of EVPOMEs pretreated with 2 nM of rapamycin was compared to the spectrum of control constructs without rapamycin pretreatment is shown in Figure 6. The ratio of the amide III band height to phenylalanine band height was always higher ($p = 0.02$) for rapamycin-treated constructs than for controls (Fig. 7a), while the clearest separation was achieved via SVD analysis (Fig. 7b).

Histology and glucose consumption

In this study, the stress applied to each group of constructs was known in advance. In the general case, where constructs are manufactured for direct implantation, this information is not available, and the EVPOMEs are classified by histological examination of the H&E-stained cell layer. Figure 8a shows Ca^{2+}- and thermally stressed specimens classified by the histological quality of the cellular layer. The specimens were classified as damaged or intact based on images of H&E-stained specimens, without knowledge of whether the specimens were stressed or nonstressed. Figure 8b shows the CH_2/phenylalanine band height ratio for discriminating specimens pooled together across batches for damaged and intact cellular layer (classified based on H&E-stained images). Using the CH_2/phenylalanine band height ratio and setting the threshold to 2.1 (the value that maximizes the sensitivity and specificity), intact and damaged specimens were classified with 82% sensitivity and 76% specificity. In comparison, plotting the CH_2/phenylalanine band height ratio as a function of stress for both heat and calcium stressing (1.8 mM or higher Ca^{2+} concentration) and setting the

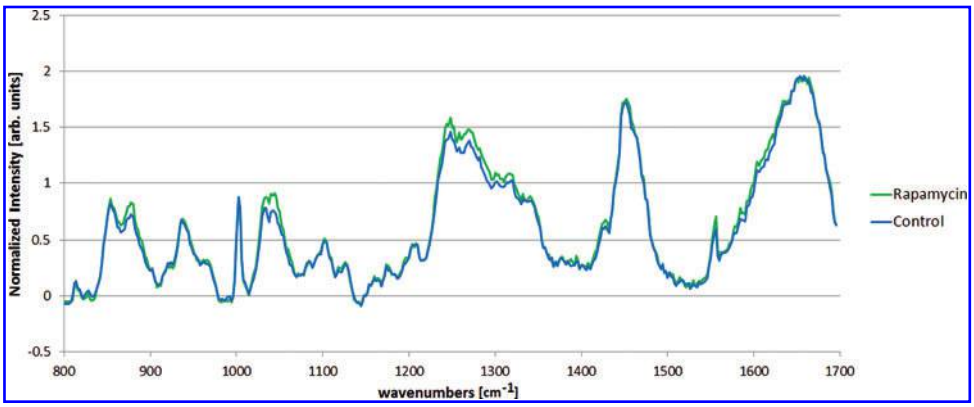

FIG. 6. Normalized Raman spectra of EVPOME exposed to rapamycin (2 nM) versus control. Color images available online at www.liebertpub.com/tec

threshold to 2.1 (see Fig. 8c), we obtained 75% sensitivity and 86% specificity for heat-stressed and 77% sensitivity and 63% specificity for Ca^{2+}-stressed specimens.

Further, glucose consumption of cells is often used as a measure of overall viability, with low glucose consumption indicating low viability of cells. Figure 8d shows glucose consumption as a function of stress, indicating that the glucose consumption was poorly correlated with stress-induced cell damage for both thermal and Ca^{2+} stressing.

Discussion

It is clear that thermal stress caused structural changes in both EVPOMEs and AlloDerm. Thermally induced protein denaturing, which changes protein secondary structure, was visible in both amide bands. However, the intensity ratio of the CH_2 deformation band to phenylalanine band was much easier to measure consistently, and is therefore proposed as a metric to establish whether or not a particular specimen had been exposed to stress.

Our analysis indicated that the CH_2-to-phenylalanine band height ratio always increased with stress for both thermal and excess Ca^{2+} stress. The ratio consistently increased more with thermal stressing than with Ca^{2+} stressing. This finding was supported by histology, which indicated greater damage as a result of thermal stressing than Ca^{2+} stressing. The CH_2-to-phenylalanine band height ratio tended to increase with the higher Ca^{2+} concentrations. By using this ratio alone, or together with the information from the other Raman bands, we can determine which constructs are most viable. Such EVPOMEs can then be used for implantation, reducing the rate of rejection due to the construct nonviability.

Further, by comparing the Raman spectra of EVPOMEs and acellular AlloDerm substrates, we were able to distinguish between the areas of EVPOMEs where the cell layer was severely disrupted. The disruption of a cell layer was at least partially responsible for the difference between stressed and nonstressed constructs.

We previously observed[21] that the intensity of the phenylalanine band decreased as a result of thermal stress, which was likely also caused by disruption of the keratin layer. The intensity of the phenylalanine band was only slightly different between stressed and nonstressed AlloDerm, a finding consistent with previously reported measurements.[20]

The results of SVD analysis confirmed differences between stressed and nonstressed EVPOME spectra. As expected, the separation between Ca^{2+} stressed and nonstressed spectra was not as well defined as in the case of thermal stress, but in both cases, the stressed/nonstressed regions were clearly identifiable, confirming that additional information is contained in amide I, amide III, and other bands.

Raman spectral changes resulting from pretreatment of the human keratinocytes with rapamycin were also observed. In that case, the ratio of the amide III band height to

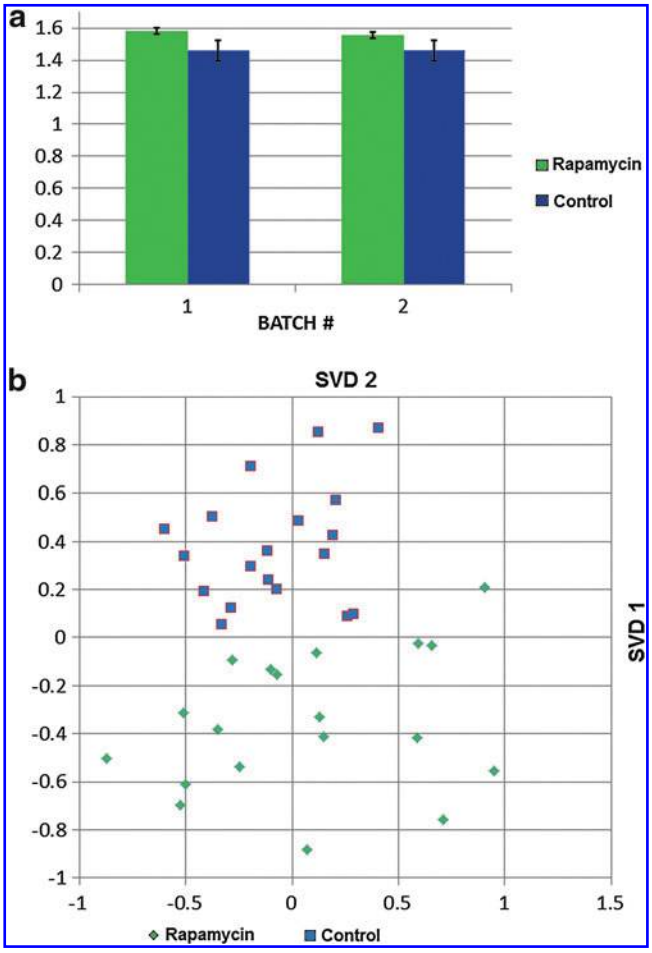

FIG. 7. **(a)** The ratio of amide III to phenylalanine band heights and **(b)** SVD separation for batches treated with rapamycin (2 nM) versus control. Color images available online at www.liebertpub.com/tec

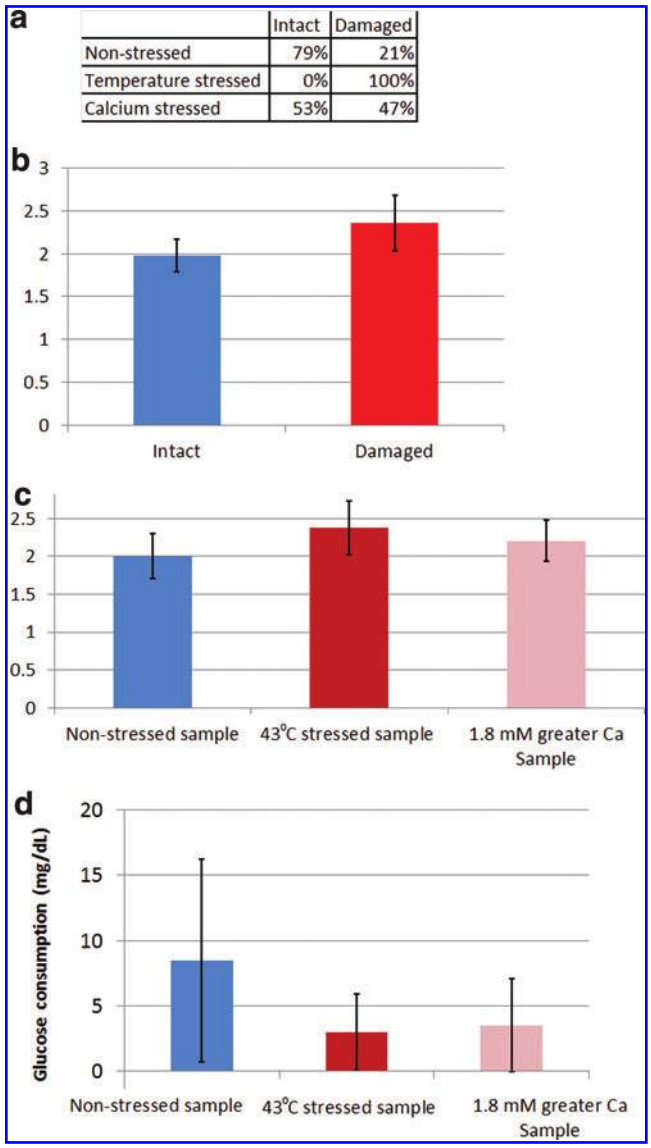

FIG. 8. Stress data for all EVPOME specimens: **(a)** cellular layer classified by histology for stressed and nonstressed specimens; **(b)** CH_2-to-phenylalanine band height ratios for intact and damaged cellular layer specimen; **(c)** CH_2-to-phenylalanine band height ratios for all batches of heat- and Ca^{2+}-stressed/nonstressed specimens, and **(d)** stress and glucose consumption, showing poor correlation between glucose consumption and stress levels. Color images available online at www.liebertpub.com/tec

phenylalanine band height was always higher for rapamycin-treated EVPOMEs, than for 1.2 mM Ca^{2+} controls.

It is unknown if our calcium ion or thermal stress protocols always result in some damage to the specimens. Either the EVPOMEs are not damaged despite being subjected to stress, or the damage is always present, but is not visible by histology. While the classification of EVPOMEs has been traditionally done by histological assessment or by measuring glucose consumption, Raman spectroscopy may provide an important noninvasive tool capable of providing complementary information to assess EVPOME cell viability.

Rapamycin treatment remains a special case because of the multiplicity of effects possible. While we have shown that Raman spectroscopy can distinguish rapamycin-treated from untreated specimens, we do not have enough information to propose specific mechanisms for the rapamycin-induced structural changes.

Conclusions

We have developed Raman spectroscopic criteria to noninvasively determine during the manufacturing process the viability of cells within the EVPOMEs. Band intensity ratios in well-defined bands can be used by themselves, or in the combination with shape changes in envelopes of overlapping bands. The clearest distinctions between stressed/nonstressed and rapamycin-treated EVPOMEs are obtained by SVD, which incorporates the greatest amount of information from their spectra.

We have also investigated the spectral changes resulting from the pretreatment of EVPOMEs with rapamycin and observed noticeable changes in the Raman spectra. We have determined the Raman metric that changes as a result of rapamycin pretreatment and show that with SVD, a clear difference between pretreated and control specimens is observable.

Acknowledgment

This work is supported in part by an NIH Grant R01 DE019431-01.

Disclosure Statement

No competing financial interests exist.

References

1. Langer, R., and Vacanti, J.P. Tissue engineering. Science **260,** 920, 1993.
2. Hoganson, D.M., Pryor, H.I. 2nd, and Vacanti, J.P. Tissue engineering and organ structure: a vascularized approach to liver and lung. Pediatr Res **63,** 520, 2008.
3. Izumi, K., Feinberg, S.E., Iida, A., and Yoshizawa, M. Intraoral grafting of an *ex vivo* produced oral mucosa equivalent: a preliminary report. Int J Oral Maxillofac Surg 32, 188, 2003.
4. Martis, C. Mucosa versus skin grafts. In: Stoelinga, P.J.W., ed., Proceedings, Consensus conference: The Relative Roles of Vestibuloplasty and Ridge Augmentation in the Management of the Atrophic Mandible. Chicago: Quintessence, 1984, p. 41.
5. Phillips, T.J. New skin for old. Arch Dermatol **134,** 344, 1998.
6. De Luca, M., Albanese, E., Megna, M., Cancedda, R., Mangiante, P.E., Cadoni, A., and Franzi, A.T. Evidence that human oral epithelium reconstituted *in vitro* and transplanted onto patients with defects in the oral mucosa retains properties of the original donor site. Transplantation **50,** 454, 1990.
7. Omura, S., Mizuki, N., Horimoto, S., Kawabe, R., and Fujita, K. A newly developed collagen/silicone bilayer membrane as a mucosal substitute: a preliminary report. J Oral Maxillofac Surg **35,** 85, 1997.
8. Raghoebar, G.M., Tompson, A.M., Scholma, J., Blaauw, E.H., Witjes, M.J.H., and Vissink, A. Use of cultured mucosal grafts to cover defects caused by vestibuloplasty: an *in vitro* study. J Oral Maxillofac Surg **53,** 872, 1995.
9. Tsai, C.-Y., Ueda, M., Hata, K., Horie, K., Hibino, Y., Sugimura, Y., Toriyama, K., and Totii, S. Clinical results of

cultured epithelial cell grafting in the oral and maxillofacial region. J Craniomaxillofac Surg **25,** 4, 1997.
10. Izumi, K., Song, J., and Feinberg, S.E. Development of a tissue-engineered human oral mucosa: from the bench to the bed side. Cells Tissues Organs **176,** 134, 2004.
11. Izumi, K., Terashi, H., Marcelo, C.L., and Feinberg, S.E. Development and characterization of a tissue-engineered human oral mucosa equivalent produced in a serum-free culture system. J Dent Res **79,** 798, 2000.
12. Izumi, K., Neiva, R., and Feinberg, S.E. Intraoral grafting of a tissue engineered human oral mucosa. Oral Craniofac Tissue Eng **1,** 103, 2011.
13. MacKay, G. Bioactive wound healing, bioaesthetics and biosurgery: three pillars of product development. Regen Med **1,** 169, 2006.
14. Sun, W., Xu, R., Hu, W., Jin, J., Crellin, H.A., Bielawski, J., Szulc., Z.M., Thiers, B.H., Obeid, L.M., and Mao, C. Upregulation of the human alkaline ceramidase 1 and acid ceramidase mediates calcium-induced differentiation of epidermal keratinocytes. J Invest Dermatol **128,** 389, 2008.
15. Stabler, C.L., Long, R.C., Sambanis, A., and Constantinidis, I. Noninvasive measurement of viable cell number in tissue-engineered constructs *in-vitro*, using 1H nuclear magnetic resonance spectroscopy. Tissue Eng **11,** 404, 2005.
16. Okagbare, P.I., and Morris, M.D. Polymer-capped fiber-optic Raman probe for non-invasive Raman spectroscopy. Analyst **137,** 77, 2012.
17. McElderry, J.-D., Kole, M.R., and Morris, M.D. Repeated freeze-thawing of bone tissue affects Raman bone quality measurements. J Biomed Opt **16,** 071407, 2011.
18. Schulmerich, M.V., Cole J.H., Kreider, J.M., Esmonde-White, F.W.L., Dooley, K.A., Goldstein, S.A., and Morris, M.D. Transcutaneous Raman spectroscopy of murine bone in vivo. Appl Spectrosc **63,** 286, 2009.
19. Dooley, K.A., Morris, M.D., McCormack, J., and Fyhrie, D.P. Stress mapping of undamaged, strained and failed regions of bone using Raman spectroscopy. J Biomed Opt **14,** 044018, 2009.
20. Lo, W.-L., Lai, J.-Y., Feinberg, S.E., Izumi, K., Kao, S.-Y., Chang, C.-S., Lin, A., and Chiang, H.K. Raman spectroscopy monitoring of the cellular activities of a tissue-engineered *ex vivo* produced oral mucosal equivalent. J Raman Spectrosc **42,** 174, 2011.
21. Khmaladze, A., Ganguly, A., Raghavan, M., Kuo, S., Cole, J.H., Marcelo, C.L., Feinberg, S.E., Izumi, K., and Morris, M.D. Raman spectroscopic analysis of human tissue engineered mucosa constructs (EVPOME) perturbed by physical and biochemical methods. Proc SPIE **8219,** 82190J, 2012.
22. Cole, J.H., Izumi, K., Feinberg, S.E., and Morris, M.D. Assessing viability and function of tissue engineered human oral mucosa with noninvasive Raman spectroscopy. Trans Orthop Res Soc **34,** 2120, 2009.
23. Izumi, K., Inoki, K., Fujimori, Y., Marcelo, C.L., and Feinberg, S.E. Pharmacological retention of oral mucosa progenitor/stem cells. J Dent Res **88,** 1113, 2009.
24. Huang, S., Bjornsti, M.A., and Houghton, P.J. Rapamycins: mechanism of action and cellular resistance. Cancer Biol Ther **2,** 222, 2003.
25. Demidenko, Z.N., Zubova, S.G., Bukreeva, E.I., Pospelov, V.A., Pospelova, T.V., and Blagosklonny, M.V. Rapamycin decelerates cellular senescence. Cell Cycle **8,** 1888, 2009.
26. Raghavan, M., Sahar, N.D., Wilson, R.H., Mycek, M.A., Pleshko, N., Kohn, D.H., and Morris, M.D. Quantitative polarized Raman spectroscopy in highly turbid bone tissue. J Biomed Optics **15,** 037001, 2010.
27. Lieber, C.A., and Mahadevan-Jansen, A. Automated method for subtraction of fluorescence from biological raman spectra. Appl Spectrosc **57,** 1363, 2003.
28. Abdi, H., and Williams, L.J. Principal component analysis. WIREs Comp Stat **2,** 433, 2010.

Address correspondence to:
Michael D. Morris, PhD
Department of Chemistry
University of Michigan
Ann Arbor, MI

E-mail: mdmorris@umich.edu

Received: May 8, 2012
Accepted: September 10, 2012
Online Publication Date: November 13, 2012

This article has been cited by:

1. Mads S. Bergholt, Michael B. Albro, Molly M. Stevens. 2017. Online quantitative monitoring of live cell engineered cartilage growth using diffuse fiber-optic Raman spectroscopy. *Biomaterials* . [CrossRef]
2. F.G. Basso, J. Hebling, C.L. Marcelo, C.A. de Souza Costa, S.E. Feinberg. 2017. Development of an oral mucosa equivalent using a porcine dermal matrix. *British Journal of Oral and Maxillofacial Surgery* **55**:3, 308-311. [CrossRef]
3. Roderick Youngdo Kim, Sam Seoho Bae, Stephen Elliott Feinberg. 2017. Soft Tissue Engineering. *Oral and Maxillofacial Surgery Clinics of North America* **29**:1, 89-104. [CrossRef]
4. E V Timchenko, P E Timchenko, L T Volova, D A Dolgushkin, P Y Shalkovskaya, S V Pershutkina, I F Nefedova. 2017. The assessment of human skin biomatrixes using raman spectroscopy method. *Journal of Physics: Conference Series* **784**, 012058. [CrossRef]
5. E V Timchenko, P E Timchenko, L T Volova, D A Dolgushkin, P Y Shalkovsky, S V Pershutkina. 2016. Detailed spectral analysis of decellularized skin implants. *Journal of Physics: Conference Series* **737**, 012050. [CrossRef]
6. Khmaladze Alexander, Kuo Shiuhyang, Kim Roderick Y., Matthews Robert V., Marcelo Cynthia L., Feinberg Stephen E., Morris Michael D.. 2015. Human Oral Mucosa Tissue-Engineered Constructs Monitored by Raman Fiber-Optic Probe. *Tissue Engineering Part C: Methods* **21**:1, 46-51. [Abstract] [Full Text HTML] [Full Text PDF] [Full Text PDF with Links]
7. Alexander Khmaladze, Joshua Jasensky, Erika Price, Chi Zhang, Andrew Boughton, Xiaofeng Han, Emily Seeley, Xinran Liu, Mark M. Banaszak Holl, Zhan Chen. 2014. Hyperspectral Imaging and Characterization of Live Cells by Broadband Coherent Anti-Stokes Raman Scattering (CARS) Microscopy with Singular Value Decomposition (SVD) Analysis. *Applied Spectroscopy* **68**:10, 1116-1122. [CrossRef]
8. Frank Winterroth, Hiroko Kato, Shiuhyang Kuo, Stephen E. Feinberg, Scott J. Hollister, J. Brian Fowlkes, Kyle W. Hollman. 2014. High-Frequency Ultrasonic Imaging of Growth and Development in Manufactured Engineered Oral Mucosal Tissue Surfaces. *Ultrasound in Medicine & Biology* **40**:9, 2244-2251. [CrossRef]